Triple Point Surface Discharge Photography in Atmospheric Gases Using Intensified High-Speed Camera System

Michail Michelarakis, David Clark, *Member*, *IEEE*, Phillip Widger, Abderrahmane Beroual, *Fellow*, *IEEE*, Ronald T. Waters, and Abderrahmane Haddad, *Member*, *IEEE*

Abstract—In this paper investigations of surface discharges using an ultraviolet (UV) intensified high-speed camera system are presented, accompanied with high frequency response and resolution current recordings. A needle-plane electrode configuration is employed for the generation of a strongly non-uniform electric field on the surface of disc-shaped insulator samples made of polytetrafluoroethylene (PTFE) or epoxy resin. The electrode arrangement is further insulated by a gaseous medium of either technical air (21% O_2/79% N_2), nitrogen (N_2) or carbon dioxide (CO_2). An alternating (AC) voltage waveform at power frequency (50Hz) is maintained at levels sufficiently below the flashover voltage corresponding to each presented case. Detailed descriptions of the technical specifications of the utilised equipment are provided for both optical and electrical measurements in the experimental set-up. The obtained results demonstrate the discharge propagation during the AC-cycle and its dependence on the insulator type and gaseous insulating medium. Individual surface discharges are captured in the microsecond range to describe the discharge morphology based on the generated current pulse and instantaneous applied voltage level. Back-discharges on the insulating disc are also discussed, and a relevant image capture is presented.

Index Terms—surface discharges, ultraviolet imaging, intensified camera, strongly non-uniform electric field, needle-plane, atmospheric gases.

I. INTRODUCTION

THE need for compact, robust and long service life gas-insulated medium- and high-voltage equipment introduces several challenging tasks during the design process of such devices. Regions of elevated electric field stress are frequently met and require special attention in the overall effort of achieving functionally reliable apparatus and components with minimised maintenance requirements and reduced risk of failure.

Common regions of high electric field stress are the imperfect interfaces between charged metal parts, solid dielectric materials and gaseous insulation, frequently referred to as triple junction points. Depending on the type of the gaseous insulation, when the critical electric field threshold is reached, the ionization processes result in the appearance of discharge activity. The energy levels of the generated discharge phenomena can be an indicator of their type and thus their severity. Such information is important in all kinds of application, from outdoor atmospheric air insulated structures to enclosed pressurised gas insulated equipment.

The development of surface discharges in the vicinity of a solid dielectric-gas interface is strongly linked to the development of enhanced electric fields at the triple junctions. From published literature [1-3], many approaches have been reported investigating the impact of gaseous medium, dielectric material, voltage wave-shape and applied voltage level on the morphology and propagation of surface discharges. With respect to the frequency response and light emission requirements, detection methods in controlled laboratory experiments are based on electrical [4] and optical techniques [5] in arrangements similar to those utilised for partial discharge and streamer detection. Various imaging techniques have also been developed [6-11], each one with its own implementation principle and practical advantages over the others, with all of them capable of providing useful outputs. The knowledge of the optical and electrical parameters of these discharges is of great interest for industrial applications for monitoring of the insulation performance and establishing proactive measures to ensure non-disruptive operation of the equipment.

This work investigates the development of surface discharges over disc-shaped solid insulator samples under strongly non-uniform electric field conditions at power frequency energisation. The insulator materials examined were pure polytetrafluoroethylene (PTFE) and epoxy resin as they are frequently met in the assemblies of medium- and high- voltage equipment and are characterised by considerably different relative permittivities (ε_r), typically 2.1 for PTFE and 3.5 for epoxy resin [1]. As gaseous insulating media, atmospheric gases were examined namely, technical air (21% O_2/79% N_2), nitrogen (N_2) of 99.998% and carbon dioxide (CO_2) of 99.8% purity. The capture of the light emitted by the generated surface discharges employed the developed UV intensified high-speed camera system synchronised with the current sensing circuit, achieving an event-based signal recording and image capturing

system. Special attention was paid to the technical specifications of the utilised accessories and equipment to maintain the maximum possible accuracy in both frequency response of the recorded signals and optical requirements of the capturing system. The obtained outputs can potentially provide an interesting insight on how accurately measured current transient pulses associated with surface discharge activity reflect in the development and morphology of such discharges in different gaseous insulating media.

II. EXPERIMENTAL SET-UP

This section describes in detail the experimental approach and set-up with focus on the technical specifications of the equipment and components used. An illustration of the full experimental set-up is shown in Fig. 1. Depending on its role, each sub-system is described within different sub-sections.

A. Electrode Configuration

In order to replicate strongly non-uniform electric field conditions, a needle-plane electrode configuration was employed. A voltage was applied to the needle electrode whilst the opposing stainless-steel plane electrode of 150mm diameter was at ground or zero potential. A disc-shaped insulator sample of 100mm diameter and thickness of either 4 or 6mm was placed between the two electrodes, with the needle probe installed perpendicularly and centred towards the insulator sample. The distance between the insulator and the needle tip was maintained at ≤0.5mm ensuring no contact between the two components. The needle is made of tungsten with 20±0.5μm tip diameter, 0.51mm shaft diameter and of 32mm length. The orientation of the configuration was horizontal with the exposed insulator surface facing the side viewport of the stainless-steel pressure chamber.

B. Current Sensing Circuit and Recording

Detection of discharge activity was performed using a fast-response shunt resistor. A 50Ω/20W load termination was connected in series with the grounded plane electrode through a coaxial surface mounted connector. An inline coaxial surge suppressor was added for overvoltage protection of the recording devices in case of unexpected flashover events. In controlled laboratory experiments, the use of a low inductance shunt resistor offers several advantages such as, high gain in the sensed signal, simple installation and operation principle and wide bandwidth range [12]. These superior properties are useful when sensing of low magnitude and fast-rising current signals is required. However, special attention should be paid to the

overvoltage protection of the recording devices and the power rating of the used components.

Prior to the tests, sensitivity checks were performed with the use of a 10-10000pC charge injector while the bandwidth range of the sensing circuit was measured with a 50Ω two-port calibrated 9kHz-6GHz vector network analyser (VNA). After the described procedure was implemented, it was ensured that the system's sensing capability of current signals of at least 10pC apparent charge, as this defined in [13], and frequency response in the range of DC-2GHz, along which attenuation of less than -3dB and close to -1dB on average, were maintained.

For the recording of the waveforms associated with the applied voltage and generated currents, a Teledyne LeCroy HDO6104, 1GHz, 2.5GS/s, 12-bit oscilloscope was used. As will be described within the next sections, different triggering arrangements were considered depending on the recording requirements of each test series.

C. High-Speed Image Capturing

The optical system, as shown in Fig. 1, comprises a UV image intensifier (UVi 1850-10-S20) ahead of a monochromatic 8-bit Photron SA5 high-speed camera. The maximum frame rate capability of the high-speed camera is 775000 frames per second (fps) at the reduced resolution of 128×24 pixels while the maximum possible resolution of 1024×1024 pixels is achievable at slower frame rates up to 7000 fps. The exposure and delay times of the of the UV image intensifier vary from 10ns to 1ms and 20ns to 10ms respectively. The optical axes of all components are collinear with the axis of the needle electrode. Discharges are observed via the side viewport of the stainless-steel pressure chamber containing a UV-grade calcium fluoride (C_aF_2) glass window. Two lenses are employed in the system: a Nikon UV-105, 105mm f/4.5 lens focuses images of the surface discharges on the insulator sample to create an intensifier input. A second Nikon 50mm f/1.4 lens enables the images of the discharge structure developed by the intensifier output to be recorded by the high-speed camera. This has enabled the time-resolved images of surface discharge development that will be presented in Section 3.

The spectral response of the image intensifier ranges from 200nm to 600nm and the UV lens is chromatically corrected in the range of 220-900nm. For all the cases, where technical air (21% O_2/79% N_2) and nitrogen (N_2) were used as insulating media, a bandpass filter was employed, effectively transmitting in the near-UV with centre wavelength at 340nm and transmission rate >80%. The UV-grade glass window provides a transmission rate on average greater than 93% within the range of 200nm to 7μm, ensuring that the light emitted from the discharge events will not be reflected.

D. High Voltage Application

In the presented test series, generation of surface discharges under AC 50Hz voltage application was examined. For that purpose, a 50kV / 3.75kVA transformer was used. Between the high voltage transformer and the test object, an RCR 3750:1 voltage divider was used to scale down the applied voltage to levels measurable by the recording devices. The applied voltage
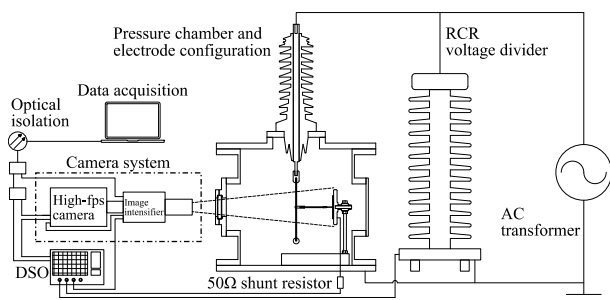

Fig. 1. Illustration of the complete experimental set-up.

3

was supplied to the electrode configuration through a 38kV AC rms rated bushing. During testing, the applied voltage was increased gradually up to the required levels, implementing the ramp rate described in [14] i.e., after 75% of the required test voltage level U was reached then approximately a 2% of U rate of rise was adopted.

Test voltage levels were specified close to 80% of the corresponding flashover (FOV) levels [4] for each insulating gas/solid insulator sample combination. This margin was maintained for the protection of both the recording and image capturing equipment. Flashover events, even if relatively short in duration, can generate light of intensity sufficient to damage the photocathode of the image intensifier and thus should be avoided. Data acquisition devices were electrically isolated from the experimental set-up through digital to optical converters.

III. TEST RESULTS AND DISCUSSION

The test series for all the cases considered were performed at least four times with a maximum of six times in case the adjustment of the optical components was found to be necessary. In that way, the risk of affecting the condition of the needle tip and/or the solid insulator surface was maintained at minimum levels. At the end of each test series both the needle electrode and the insulator sample were replaced. The presented results were chosen from a wide range of obtained data with the main criterion being the repeatability of the generated outputs.

The detected surface discharges are classified into two main categories depending on the polarities of the recorded current pulse and the applied AC waveform for a specific instant of time on the AC-cycle. As reference, an example of a full AC-cycle recording is shown in Fig. 2. When the current pulse and the applied voltage have the same polarity, then it is assumed that a forward discharge had taken place. In contrast, when they are of opposite polarity, a back-discharge had occurred [6, 15], as can be observed in regions (b) and (d) identified in Fig. 2. Positive and negative forward discharges are those taking place during the positive and negative half-cycles of the sinusoidal waveform, respectively.

A. Long Exposure Time Captures

High resolution voltage and current recordings for different insulator samples and atmospheric insulating gases were reported by the authors in [4]. For all the described cases during the positive half-cycle, most of the discharge activity was observed during the rising slope of the applied voltage and before reaching its peak value. Fig. 3 shows the case of PTFE of 4mm thickness immersed in technical air (21% O_2/79% N_2) at 1 bar absolute pressure. Generated surface discharges are presented in a sequence of frames each one corresponding to 950μs exposure time of the intensifier photocathode. The time window for each frame equals the sum of the exposure time and the approximated processing time of the capturing and recording devices, roughly approaching, and not exceeding, 1ms in total. The added white dashed circle indicates the edges of the disc-shaped insulator sample. The time division between the vertical grid lines on the measured waveforms (Fig. 3(e)) represents approximately the time window of successive frames. Considering that each discharge event develops in the sub-microsecond time scale, the emitted light from different discharge events might reasonably overlap within the same time window. The propagation of discharges is radial, initiated from the centre of the sample where the charged needle tip is located, expanding in all directions on the insulator sample surface away from the central needle tip.

Following the same approach, the same insulator sample type is shown in Fig. 4, this time immersed in nitrogen (N_2) at 1 bar absolute pressure. Again, it can be clearly seen that as the voltage increases from the zero-crossing point towards the peak value of the positive AC half-cycle, the discharges appear to cover longer distances on the insulator surface. The rms applied voltage in this case was lower compared to that used in Fig. 3. However, for both cases it was 80% of the corresponding rms FOVs.
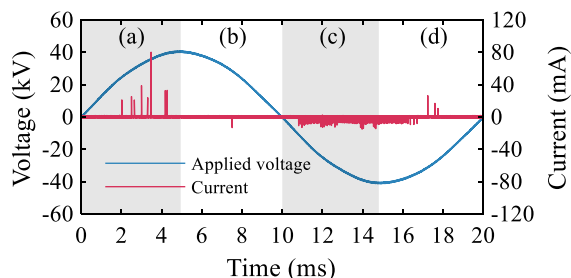

(a)

(b)

(c)

(d)

(e)

Fig. 2. Example of full 50Hz AC-cycle recording of the applied voltage and generated current. Here, the case of PTFE 6mm thickness in technical air at 1 bar absolute pressure is shown. Regions (a), (b), (c) and (d) are distinguished based on the polarity and slope of the applied sinusoidal voltage.

Fig. 3. Surface discharge development during the rising slope of the positive half-cycle of the applied AC voltage for the case of PTFE 4mm thickness in technical air (21% O_2/79% N_2) at 1 bar absolute pressure and rms applied voltage around 80% (28.81kV) of the corresponding rms FOV: (a) 0-1ms (b) 1-2ms (c) 2-3ms (d) 3-4ms and (e) voltage and current measurements

Fig. 4. Surface discharge development during the rising slope of the positive half-cycle of the applied AC voltage for the case of PTFE 4mm thickness in nitrogen (N_2) at 1 bar absolute pressure and rms applied voltage around 80% (16.61kV) of the corresponding rms FOV: (a) 0-1ms (b) 1-2ms (c) 2-3ms (d) 3-4ms and (e) voltage and current measurements.
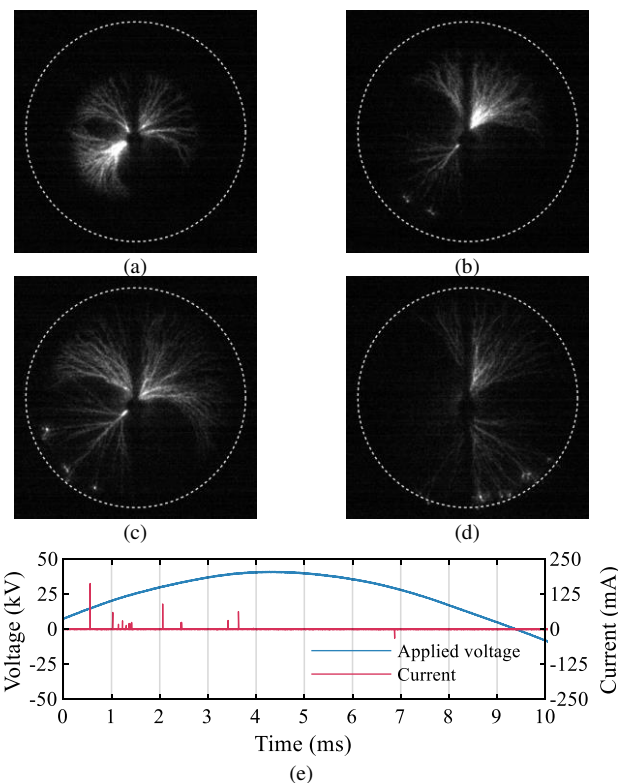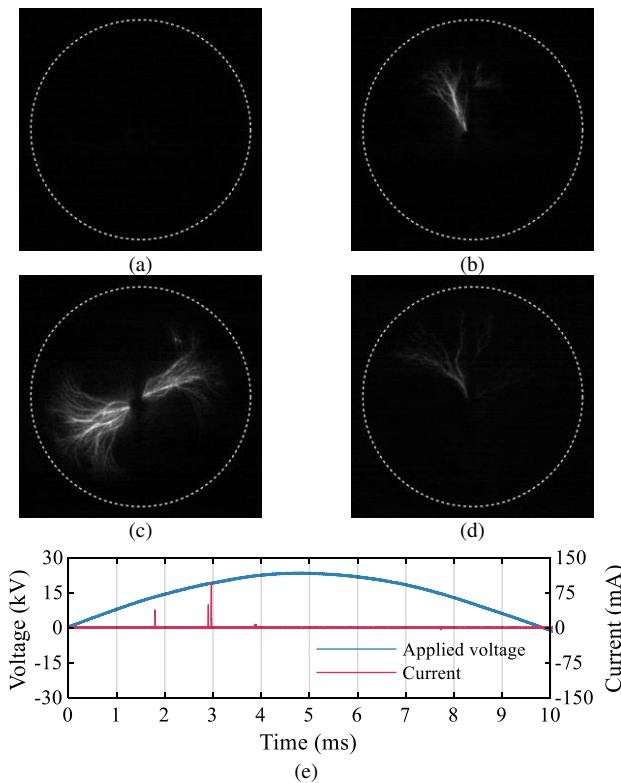

Fig. 5. Surface discharge development during the rising slope of the positive half-cycle of the applied AC voltage for the case of PTFE 4mm thickness in carbon dioxide (CO_2) at 0.5 bar absolute pressure and 19.31kV rms applied voltage: (a) 0-1ms (b) 1-2ms (c) 2-3ms (d) 3-4ms and (e) voltage and current measurements.

The capture of positive polarity forward discharges in technical air and nitrogen was found to be easier compared to the case of carbon dioxide (CO_2) and for voltage levels up to 80% of the corresponding rms FOVs. A possible explanation is that, in CO_2, discharges in the form of a streamer channel begin to develop on the surface of the insulator samples at voltage levels closer to flashover. The pulses detected with the current sensing circuit are of relatively low magnitude and they are likely to represent discharges which propagated over very short distances around the needle tip and within a small area around the electrode. This can be an indication that CO_2 can stunt streamer growth in high field regions more effectively compared to the other gases considered in this investigation. The captured images at 1 bar absolute pressure consisted mainly of very bright points, of a few pixels each, spread around the centre area of the disc insulator sample. It is unclear whether these small bright points are a result of light emitting electronic processes or noise induced on the photocathode of the image intensifier. For the test series involving CO_2, the pressure was decreased to 0.5 bar absolute, effectively reducing the density of charge carriers and insulation strength of the gas within the filled volume. The applied voltage was gradually increased up to a level when current pulses of relatively high magnitude were detectable during the positive half-cycle. The corresponding captures are shown in Fig. 5. It is worth noting that, for these test series, the intensifier relative gain values were approaching 70%, much higher than for the cases of technical air and N_2 (40-45%) considering the exponential gain transfer efficiency of the image intensifier photocathode.
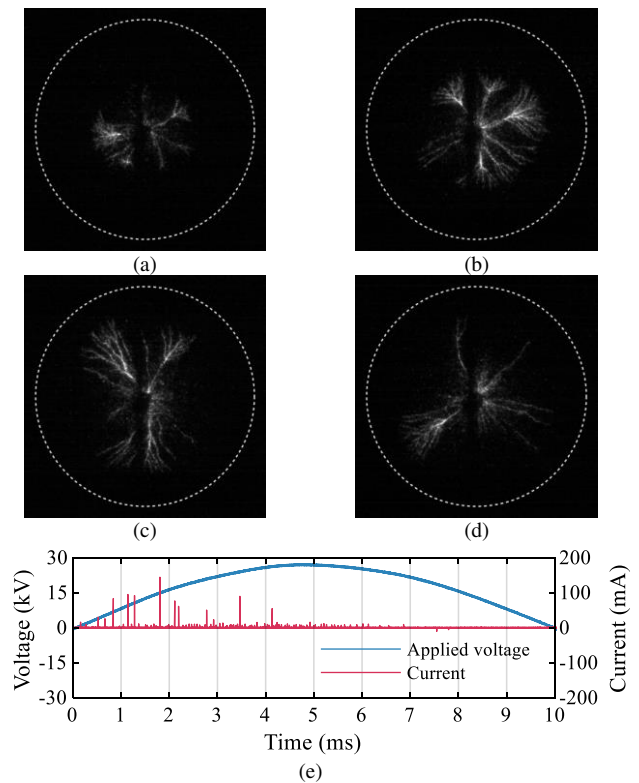
Fig. 6 shows, the captures for PTFE of 6mm thickness in technical air at 1 bar absolute pressure. The applied voltage was of almost the same level as for the case in Fig. 3 since no flashover events were observed within the maximum allowed applied voltage levels for that particular gaseous medium/solid insulator sample combination [4]. Similarities in the morphology of the generated discharges for 4mm and 6mm thick samples are observable, indicating its dependence primarily on the gaseous insulating medium type. It is worth commenting that, again, the propagation length of the discharges appears to be very close to the insulator edges with very luminous small regions at the end of the discharge channel for both cases. This is more observable in Fig. 6(c), in regions where the branches on the tips of discharge channels are less dense. It could be said that the electric field is locally elevated around the tip of the discharge channel which is further enhanced as the same discharge approaches the ground potential electrode. For the voltage levels considered, samples of thicknesses 4mm and 6mm, resulted in similar discharge patterns for the three different gases utilised and no clear observations can be made at this stage regarding the effect of the sample thickness on the morphology of the discharges. However, it is clearly observed that discharge activity is slightly denser in Fig. 3(e) compared to Fig. 6(e) although larger time samples and a statistical study is required for confidence in these noted observations [4].

The use of an insulator sample made of a material of higher relative permittivity appears to introduce more noticeable variations in the output captures. Fig. 7 summarises the recordings for epoxy resin (ε_{ER} = 3.5) of 4mm thickness in
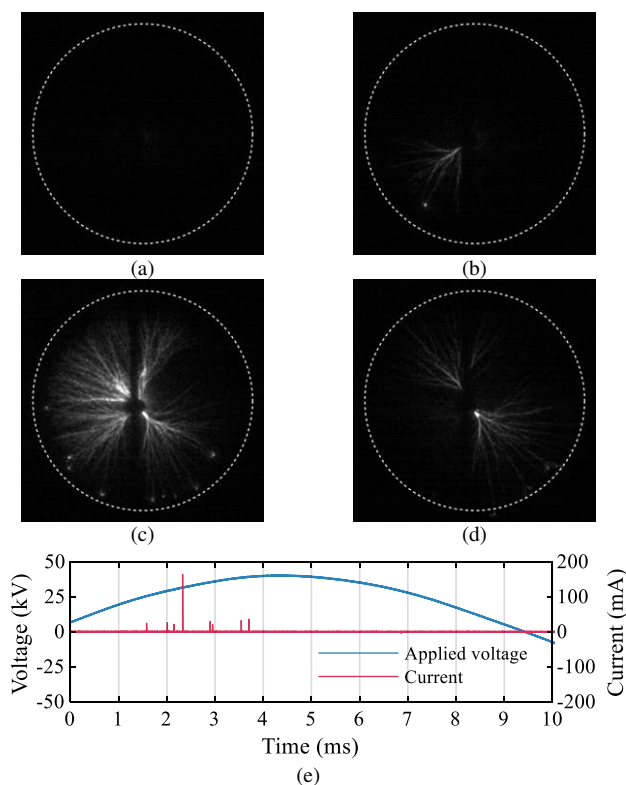
Fig. 6. Surface discharge development during the rising slope of the positive half-cycle of the applied AC voltage for the case of PTFE 6mm thickness in technical air (21% O_2/79% N_2) at 1 bar absolute pressure and 28.58kV rms applied voltage: (a) 0-1ms (b) 1-2ms (c) 2-3ms (d) 3-4ms and (e) voltage and current measurements.
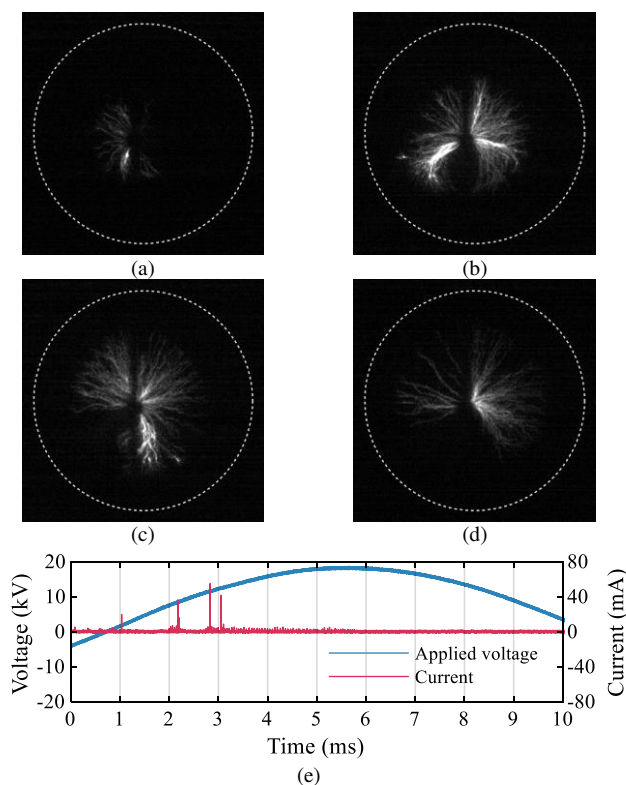

Fig. 7. Surface discharge development during the rising slope of the positive half-cycle of the applied AC voltage for the case of epoxy resin 4mm thickness in nitrogen (N_2) at 1 bar absolute pressure and rms applied voltage around 80% (13.13kV) of the corresponding rms FOV: (a) 1-2ms (b) 2-3ms (c) 3-4ms (d) 4-5ms and (e) voltage and current measurements.

nitrogen (N_2). Again, the applied rms voltage was 80% of the expected FOV. Compared to the results of Fig. 4, it can be seen that generated discharges are spread over larger circular regions, even when the applied sinusoidal voltage is close to its zero-crossing, maintaining at the same time the tendency to expand as the applied voltage level approaches its peak value. Similar variations are observed with technical air and CO_2 when an epoxy resin sample is used instead of the lower relative permittivity PTFE (ε_{PTFE} = 2.1). Such a behaviour can be attributed to the fact that the coupling capacitance between the charged and grounded electrodes is modified by the presence of a material of higher relative permittivity, extensively documented by the authors in [1] and [2]. Additionally, the rms applied voltages for the examples of Fig. 4 and Fig. 7 were different, 16.61kV and 13.13kV respectively, as they were expressed relevant to their FOVs and consequently different electric field magnitudes were generated at the needle tip. In absolute values, the margin in the case of PTFE was around 4.2kV below the flashover, while it was around 3.3kV for epoxy resin [4]. Further investigation is needed of how the field displacement effect contributes to the generation and propagation of discharge activity around the needle tip on the surface of the insulator, from the inception until the final flashover.

B. Short Exposure Time Captures

The capture of individual positive polarity forward discharges was performed using an event-based, pattern generated, triggering technique ensuring that each current pulse detected by the current sensing circuit will be captured in a single frame.

The exposure time of the UV intensifier was set to 20µs with sufficient time margins set in the high-speed camera considering nanosecond level time delays for the synchronisation of the devices. Negative polarity discharges during the negative half-cycle of the applied AC voltage waveform, for the presented vertical resolution (V/div) of the recording device, were electrically detected for the cases where technical air or carbon dioxide were used as gaseous insulating media [4]. However, no discharge channels were captured over the insulator sample surfaces for the applied voltage levels examined during the described test series, indicating that the negative forward discharges appear locally on the needle tip and within a very small region around it on the insulator surface. Observations regarding the longer propagation length of positive discharges compared to negative were also reported in [6].

Fig. 8 presents selected captures of individual surface discharge events. Below each captured frame, the corresponding current measurements are included. On the same plot, the apparent charge is calculated by integrating the current pulse over the presented time interval. The last part of this group of figures (Fig. 8(d)) shows an illustration of the positive half-cycle for a 50Hz sinusoidal waveform, indicating approximately the time points where the current pulses appear relevant to the applied voltage. For all three cases, the rms applied voltage is 80% of the expected FOV and thus the illustrated waveform is shown normalised to its peak value.

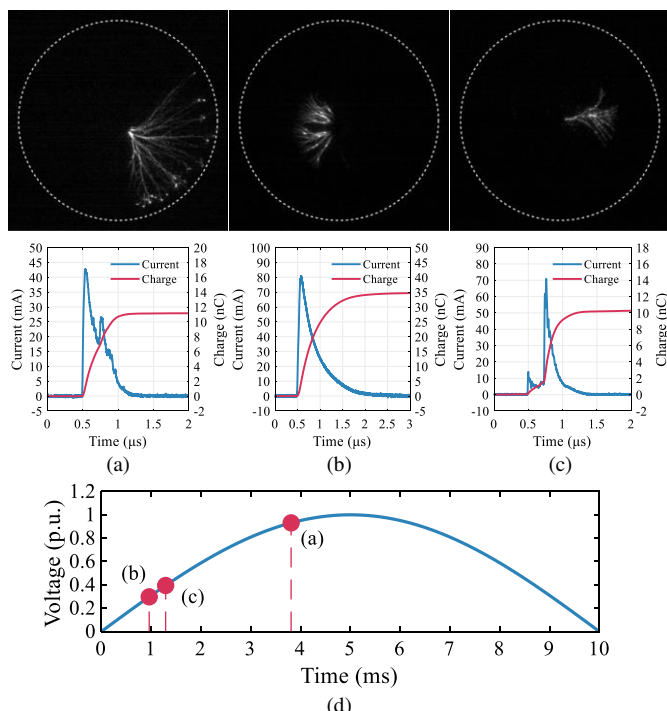The current pulse of Fig. 8(a) is of relatively low magnitude

Fig. 8. Short exposure (20μs) capturing of surface discharge events: (a) epoxy resin 6mm in technical air at 1 bar absolute (b) epoxy resin 6mm in nitrogen (N_2) at 1 bar absolute, (c) PTFE 4mm in carbon dioxide (CO_2) at 0.5 bar absolute and (d) illustration of 50Hz positive half-cycle showing the approximate location of the discharges within the time domain.

however, it appears to extend its propagation up to the edge of the disc insulator and towards the grounded plane. The same observation can be made from Fig. 3 and Fig. 6 where technical air was also tested but with different insulator sample types. Examining both the long exposure frames and the individual pulse of Fig. 8(a), it could be said that higher magnitude current peaks correspond to a greater spread of discharge activity on the circular top surface of the insulator. However, the information from the recorded current pulse cannot alone be an indicator of the propagation length of the corresponding discharge and the time, or phase, stamp within the AC-cycle is required. While approaching the peak value of the applied voltage, the positively charged insulator [7] will accumulate even more positive charge on its surface. This will be a result of the positive polarity discharge activity which appeared in the previous time instants and the drift movement of the high mobility electrons towards the positively charged needle, leaving behind the slowly moving positive ions [8, 9]. The electric field on the insulator surface is dependent on both the externally generated electric field and the field generated by the presence of the created space charge. Such behaviour has greater impact especially for relatively slowly varying applied voltages, such as at 50/60Hz power frequency.

The current pulse of Fig. 8(b) takes place at a time point close to the zero-crossing of the sinusoidal applied voltage and is of relatively high peak value. As seen from the captured frame, the discharge does not propagate to a great distance, agreeing with the pattern shown in all the previous captures. As the instantaneous voltage level increases, within the same AC-

cycle, the generated discharges are likely to propagate further on the insulator surface. For CO_2 at 0.5 bar absolute, shown in Fig. 8(c), the morphology of the discharge has similarities with the captures of Fig. 5, i.e., an initial channel begins to propagate from the needle tip location and as it extends it tends to spread in smaller branches. The current pulse comprises of two superimposed pulses, both developed in the sub-microsecond time scale, indicating a possible two-step process.

Fig. 9 includes recorded frames and measurements obtained from the same test series as those presented in Fig. 8. For all the cases, a correlation can be clearly seen between current pulse characteristics and voltage level, at these particular short time intervals. The difference is more noticeable by comparing Fig. 8(b) and Fig. 9(b). Although occurring at a higher external field, a pulse of less than half the magnitude and apparent charge propagates further on the surface. Compared to Fig. 8(a), Fig. 9(a) illustrates a discharge event of lower magnitude appearing earlier in the positive AC half-cycle and for which both the spread of the branches is narrower and the extension range is shorter. The test series with CO_2 were performed at a lower pressure level and cannot be easily directly compared with the other cases presented. However, a longer extension of the discharge region of Fig. 9(c) compared to Fig. 8(c) is noticed.

Back-discharges have been reported in previous works where different optical techniques [6, 7, 10, 11] were used. For the presented series of tests, these kinds of discharges appear to be of relatively high magnitude on some occasions. However, they do not propagate over distances far from the needle tip, as happens with positive forward discharges, and thus their
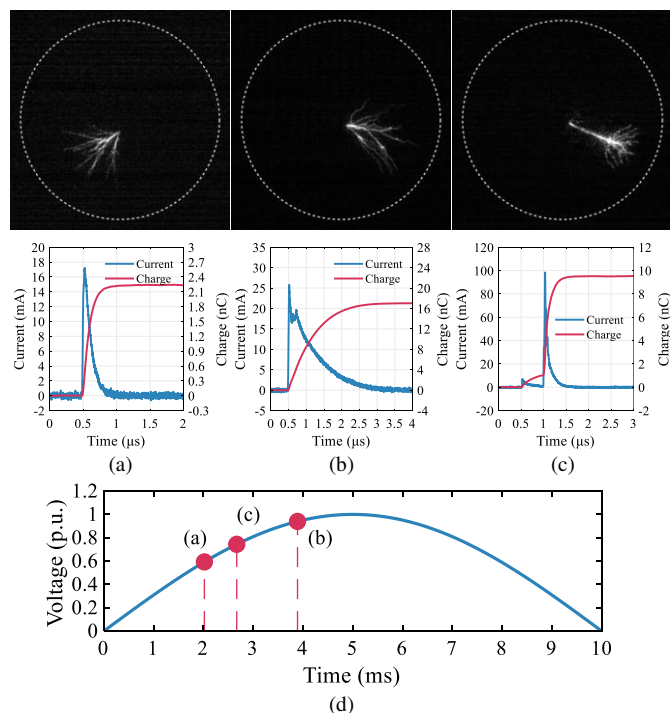

Fig. 9. Short exposure (20μs) capturing of surface discharge events: (a) epoxy resin 6mm in technical air at 1 bar absolute (b) epoxy resin 6mm in nitrogen (N_2) at 1 bar absolute, (c) PTFE 4mm in carbon dioxide (CO_2) at 0.5 bar absolute and (d) illustration of 50Hz positive half-cycle showing the approximate location of the discharges within the time domain.

capture is difficult. Fig. 10 shows an example of positive polarity back-discharge, occurring during the rising slope (from peak to zero-crossing) of the negative half-cycle of the applied voltage (see region (d) in Fig. 2 for reference) for PTFE of 4mm thickness in nitrogen (N_2). Regardless of the polarity, back-discharges have been correlated with the charge memory effect [6] and the presence of accumulated surface charge. In [15] a similar observation was made with the application of a positive semi-square voltage and the back-discharge appearing after the voltage had reached zero volts.

Characteristics of individual current pulses can provide information related to the gaseous medium [16]. However, investigating surface discharges requires that the impact of the insulator sample be considered [17, 18]. As happens with partial discharge studies, large datasets will lead to more convergent observations during the statistical study of such phenomena while at the same time attention shall be paid to the parameters under observation and the correlation between them [19, 20].

IV. CONCLUSIONS

In this paper, captures using a recently developed ultraviolet (UV) intensified high-speed capture system combined with high-frequency and high-resolution measurements were presented. Tests were performed using atmospheric insulating gases, namely technical air (21% O_2/79% N_2), nitrogen (N_2) and carbon dioxide (CO_2). Disc-shaped insulator samples made of polytetrafluoroethylene (ε_{PTFE} = 2.1) and epoxy resin (ε_{ER} = 3.5) of 4mm and 6mm thicknesses were used, and selected results were presented to demonstrate observed differences in the experimental outputs.

Most of the presented captures were performed entirely within the UV range with the use of a bandpass filter installed on the camera system, except for the case of CO_2 because of the lower luminosity of the discharge events. Long and short exposure time trigger set-ups were used for the synchronisation of the waveform recording and image capturing systems. The applied voltage was maintained at 80% of the expected FOVs for the overvoltage protection of the used equipment.

Obtained results include capturing and recording of positive polarity discharges during the positive half-cycle of the applied 50Hz AC voltage, individual current pulses, and back-discharge activity. Through capturing of consecutive long exposure frames, it was shown that the propagation length of discharges increases with the increase of the applied voltage magnitude,
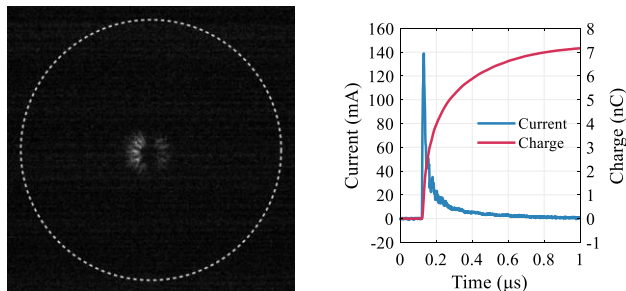

Fig. 10. Capture of positive polarity back-discharge for PTFE 4mm thickness in nitrogen (N_2) at 1 bar absolute pressure and rms applied voltage around 80% (16.61kV) of the corresponding rms FOV. The presented discharge event appeared at around -14.10kV.

from the zero-crossing point towards its peak value. Individual discharge captures helped understanding how applied voltage and generated current reflect to the morphology and propagation of the discharge event. It was shown that the current pulse alone cannot be an indicator of the appeared discharge morphology, although combined with the time or phase angle of occurrence, it can provide a clearer understanding.

The subdivision of AC surface discharges in each half-cycle into forward discharges followed by back-discharges was introduced in the previous section. The present tests allow further understanding on these discharges:

(a) Positive forward discharges are observed to occur as a successive series of separate streamer channels, sometimes traversing the insulator disc radius of 50mm, with each discharge current rise being established within some nanoseconds depending on the gaseous medium. The current duration is relatively long, in some cases up to the microsecond range, and the charge transported can be tens of nC. It is to be noted that a significant advantage of the needle-insulator-ground plane configuration used in these tests is the achievement of close coupling of the ground plane with the surface space charge of the streamers. As a result, the magnitude of the apparent charge at the planar surface of the insulator samples is much more closely representative of the real surface charge created by the streamers than can be in the case of conventional partial discharge measurement.

(b) Negative forward discharge streamers were not captured indicating that their propagation does not extend to sufficient distances to be captured by the intensified camera system. When these discharges are detectable, they are of considerably lower magnitude and have different current pulse characteristics confirming the reported results.

(c) The positive back-discharges which are often recorded are streamers initiated by the reversal of surface field by the positive ions of the forward discharges. These are characterized by a distinctive short range and low charge flow.

(d) Similar surface charge properties to those of positive back-discharges are also created by the negative ions deposited on the surface in the negative forward discharge streamers. Although of too low visibility to be recorded here, the long duration of these discharges is the cause of negative back-discharges.

Successive stages of the development of surface discharge phenomena, ranging from their inception up to the withstand levels of the insulation will potentially provide a complete overview of the surface discharge mechanisms. Larger measurement datasets, either time- or phase-resolved or both, in a test arrangement similar to the one presented in this work, will contribute to more converging observations. Imaging techniques, when combined with accurately performed measurements can provide a very interesting insight on the understanding of such phenomena.

REFERENCES

[1] F. Sadaoui and A. Beroual, "AC creeping discharges propagating over solid-gas interfaces," *IET Sci. Meas. Technol.*, vol. 8, no. 6, pp. 595-600, Nov. 2014.

[2] F. Sadaoui and A. Beroual, "DC creeping discharges over insulating surfaces in different gases and mixtures," *IEEE Trans. Dielectr. Electr. Insul.*, vol. 21, no. 5, pp. 2088-2094, Oct. 2014.

[3] A. Beroual, M.L. Coulibaly, O. Aitken and A. Girodet, "Investigation on creeping discharges propagating over epoxy resin and glass insulators in the presence of different gases and mixtures," *Eur. Phys. J. Appl. Phys.*, vol. 56, no. 3, Nov. 2011.

[4] M. Michelarakis, P. Widger, A. Beroual and A. Haddad, "Electrical detection of creeping discharges over insulator surfaces in atmospheric gases under AC voltage application," *Energies*, vol. 12, no. 15, p. 2970, Aug. 2019.

[5] F. H. Kreuger, P. H. F. Morshuis, and W. A. Sonneveld, "Optical detection of surface discharges," *IEEE Trans. Dielectr. Electr. Insul.*, vol. 23, no. 3, pp. 447-449, Jun. 1988.

[6] Y. Zhu, T. Takada, Y. Inoue and D. Tu, "Dynamic observation of needle-plane surface discharge using the electro-optical Pockels effect," *IEEE Trans. Dielectr. Electr. Insul.*, vol. 3, no. 3, pp. 460-468, Jun. 1996.

[7] Y. Zhu T. Takada, K. Sakai and D. Tu, "The dynamic measurement of surface charge distribution deposited from partial discharge in air by Pockels effect technique," *J. Phys. D: Appl. Phys.*, vol. 29, no. 11, pp. 2892-2900, Nov. 1996.

[8] Y. Murooka and S. Koyama, "A nanosecond surface discharge study in low pressures," *J. Appl. Phys.*, vol. 50, no. 10, pp. 6200-6206, Oct. 1979.

[9] H. -B. Mu *et al*, "Investigation of surface discharges on different polymeric materials under HVAC in atmospheric air," *IEEE Trans. Dielectr. Electr. Insul.*, vol. 18, no. 2, pp. 485-494, Apr. 2011.

[10] Y. Murooka and S. Koyama, "Nanosecond surface discharge study by using Dust figure techniques," *J. Appl. Phys.*, vol. 44, no. 4, pp. 1576-1580, Apr. 1973.

[11] Y. Murooka, T. Takada, and K. Hiddaka, "Nanosecond surface discharge and charge density evaluation part I: review and experiments," *IEEE Elect. Insul. Mag.*, vol. 17, no. 2, pp. 6-16, Mar.-Apr. 2001.

[12] S. Ziegler, R. C. Woodward, H. H. Iu and L. J. Borle, "Current sensing techniques: a review," *IEEE Sensors J.*, vol. 9, no. 4, pp. 354-376, Apr. 2009.

[13] High-voltage test techniques. Partial discharge measurements, BS EN 60270:2001+A1:2016, 2001-08-15.

[14] High-voltage test techniques - Part 1: General definitions and test requirements, BS EN 60060-1:2010, 2011-02-28.

[15] P. Fu, Z. Zhao, X. Li, X. Cui, T. Wen and S. Mo, "Surface discharge characteristics and initiation mechanism of PEEK in nitrogen under semi-square voltage," *AIP Adv.*, vol. 8, no. 7, p. 075322, Jul. 2018.

[16] H. Okubo, N. Hayakawa, and A. Matsushita, "The relationship between partial discharge current pulse waveforms and physical mechanisms," *IEEE Elect. Insul. Mag.*, vol. 18, no. 3, pp. 38-45, May-Jun. 2002.

[17] J. Kindersberger and C. Lederle, "Surface charge decay on insulators in air and sulfurhexafluorid - part I: simulation," *IEEE Trans. Dielectr. Electr. Insul.*, vol. 15, no. 4, pp. 941-948, Aug. 2008.

[18] J. Kindersberger and C. Lederle, "Surface charge decay on insulators in air and sulfurhexafluorid - part II: measurements," *IEEE Trans. Dielectr. Electr. Insul.*, vol. 15, no. 4, pp. 949-957, Aug. 2008.

[19] R. J. Van Brunt, E. W. Cernyar, and P. von Glahn, "Importance of unraveling memory propagation effects in interpreting data on partial discharge statistics," *IEEE Trans. Dielectr. Electr. Insul.*, vol. 28, no. 6, pp. 905-916, Dec. 1993.

[20] M. G. Danikas, N. Gao, and M. Aro, "Partial discharge recognition using neural networks: a review," *Elect. Eng.*, vol. 85, no. 2, pp. 87-93, Jan. 2003.